

Tropical cyclone convection: the effects of ambient vertical vorticity

Ulrike Wissmeier and Roger K. Smith*

Meteorological Institute, University of Munich, Germany

*Correspondence to: R. K. Smith, Meteorological Institute, University of Munich, Theresienstrasse 37, 80333 Munich, Germany. E-mail: roger.smith@lmu.de

We present idealized numerical model experiments to isolate and quantify the influence of ambient vertical vorticity on the dynamics of deep convection, such as that in the inner-core region of a tropical depression. The vertical vorticity is represented either by a uniform horizontal shear, a uniform solid-body rotation, or a combination of both. We show that the growing convective cells amplify locally the ambient rotation at low levels by more than an order of magnitude and that this vorticity, which is produced by the stretching of existing ambient vorticity, persists long after the initial updraught has decayed. Significant amplification of vorticity occurs even for a background rotation rate typical of the undisturbed tropical atmosphere and even for clouds of only moderate vertical extent. This finding has important implications for tropical cyclogenesis and provides a basis for a unified theory of tropical cyclogenesis and tropical cyclone intensification.

The presence of ambient vertical vorticity *reduces* the updraught strength, slightly more when the vorticity is associated with horizontal shear than when it is associated with solid-body rotation on account of enhanced entrainment. The reduction of the updraught strength can be attributed to the reduction of the lateral inflow by the centrifugal and Coriolis forces. Despite the significant amplification of vorticity, the sum of the centrifugal and Coriolis forces is mostly small compared with the lateral pressure gradient. Thus, at the level of background rotation studied, the Rossby elasticity effects in the updraught postulated by Montgomery *et al.* are not large, but may be important for higher levels of background rotation. The simulations ignore several processes that are likely to be important in reality, such as ambient vertical shear and surface friction, but they provide important benchmark calculations for interpreting the additional complexity arising from the inclusion of these effects.

Copyright © 2011 Royal Meteorological Society

Key Words: tropical cyclone; vortical hot towers; rotating deep convection

Received 28 August 2010; Revised 27 January 2011; Accepted 4 March 2011; Published online in Wiley Online Library 23 May 2011

Citation: Wissmeier U, Smith RK. 2011. Tropical cyclone convection: the effects of ambient vertical vorticity. *Q. J. R. Meteorol. Soc.* 137: 845–857. DOI:10.1002/qj.819

1. Introduction

There is a mounting evidence that the genesis and intensification of tropical cyclones is an intrinsically non-axisymmetric process involving the formation and mutual

interaction of rotating, deep convective clouds. The early ideas on the subject emerged from pioneering theoretical studies of vortex Rossby waves by Montgomery and colleagues in the late 1990s and early years of the twentieth century. A review of this work and a list of references is

given by Nguyen *et al.* (2008, henceforth M1). Detailed observational evidence for the occurrence of rotating deep convection has been acquired only recently and will be reviewed in section 1.2 below. We begin with a summary of some of the key modelling studies.

1.1. Modelling studies

A notable milestone in demonstrating the role of rotating deep convection on tropical cyclogenesis was the paper by Hendricks *et al.* (2004). These authors analyzed a high-resolution, near-cloud-resolving, numerical simulation of hurricane *Diana* (1984) using a 3 km horizontal grid spacing. Their aim was to understand the vorticity dynamics of the incipient organizational phase of the storm. The study indicated that the preferred convective structures have updraughts with a horizontal scale on the order of 10–30 km and, because they grow in a cyclonic vorticity-rich environment, they have intense vertical vorticity in their cores. Hendricks *et al.* coined the term vortical hot towers (VHTs) to describe these clouds.

In a subsequent numerical study, Montgomery *et al.* (2006) examined the role of VHTs in the metamorphosis of an idealized mid-level cyclonic mesoscale convective vortex to a tropical depression. Using a 2 km or 3 km horizontal grid spacing on the fine mesh of the model, they showed that, in a conditionally unstable environment, a single mid-level cyclonic vortex can undergo a metamorphosis to a tropical depression vortex on meteorologically realistic time-scales (order 1–2 days). Again within the convectively unstable and vorticity-rich environment provided by the initial embryo vortex, horizontally small-scale cyclonic VHTs emerge as the dominant coherent structures. The article describes how the vorticity dynamics of the VHTs contributes to the system-scale spin-up process.

A similar idealized numerical study, described in M1, was designed to investigate the dynamics of tropical cyclone amplification in three dimensions and the predictability of the ensuing flow. This study focused on the prototype amplification problem, which considers the evolution of a prescribed, initially cloud-free, axisymmetric, baroclinic vortex on an f -plane. Unlike that in the model of Montgomery *et al.*, the initial vortex was warm-cored with a maximum tangential wind speed of 15 m s^{-1} located at the surface. As soon as model convection develops, the flow becomes highly asymmetric even though the problem as posed is essentially axisymmetric and the flow evolution is again dominated by VHTs, which have a stochastic component. As in the calculations of Hendricks *et al.* and Montgomery *et al.*, it is the progressive segregation, merger and axisymmetrization of these towers and the low-level convergence they generate that are fundamental to the spin up of the system-scale vortex. A similar process of evolution occurs even in a tropical cyclone model with minimal vertical resolution (Shin and Smith, 2008).

The only other theoretical studies of tropical cyclone convection that we are aware of are those of McCaul and Weissman (1996) and Rozoff (2007). McCaul and Weissman (1996) carried out numerical simulations of supercell storms in the environment of landfalling hurricanes. They showed that supercell storms are possible, even though their buoyancy is limited because ambient lapse rates are close to moist adiabatic. Further, the updraughts generally reach a peak intensity at low levels, often around 2 km above

the surface. They argued that, although the amplitude of parcel buoyancy is often small in hurricane environments, its concentration in the strongly sheared lower troposphere promotes the development of perturbation pressure minima comparable to those seen in Great Plains supercells. Surprisingly, they did not consider the effects of enhanced vertical vorticity in the hurricane environment.

Rozoff (2007) carried out a series of numerical experiments on an f -plane to explore, *inter alia*, the effects of uniform horizontal shear on deep convection. He showed that horizontal shear is generally detrimental to the development of convection, and quantified the effect of different amounts of shear on the strength and structure of the convection.

1.2. Observational studies

The discovery of VHTs in three-dimensional numerical model simulations of tropical cyclogenesis and tropical cyclone intensification has motivated efforts to document such structures in observations. Two early studies were those of Reasor *et al.* (2005), who used airborne Doppler radar data to show that VHTs were present in the genesis phase of hurricane *Dolly* (1996), and Sippel *et al.* (2006), who found evidence for VHTs during the development of tropical storm *Alison* (2001). It was not until very recently that Houze *et al.* (2009) presented the first detailed observational evidence of VHTs in a depression that was intensifying and which subsequently became hurricane *Ophelia* (2005). The updraught that they documented was 10 km wide and had vertical velocities reaching $10\text{--}25 \text{ m s}^{-1}$ in the upper portion of the updraught, the radar echo of which reached to a height of 17 km. The updraught was contiguous with an extensive stratiform region on the order of 200 km in extent. Maximum values of vertical vorticity averaged over the convective region during different fly-bys of the convective region were on the order of $5\text{--}10 \times 10^{-4} \text{ s}^{-1}$ (Houze *et al.*, 2009, Figure 20).

Bell and Montgomery (2010) analysed airborne Doppler radar observations from the recent Tropical Cyclone Structure 2008 field campaign in the western North Pacific and found the presence of deep, buoyant and vortical convective features within a vertically sheared, westward-moving pre-depression disturbance that later developed into typhoon *Hagupit*. Raymond and López-Carillo (2011) carried out a similar analysis of data from the same field experiment, in their case for different stages during the intensification of typhoon *Nuri*, and provided further evidence for the existence of VHT-like structures.

Guimond *et al.* (2010) described observations including analyses of airborne Doppler radar measurements of deep convective bursts preceding a period of rapid intensification of hurricane *Dennis* (2005) and during the mature stage of this storm. They reported finding convective cells with updraughts of 20 m s^{-1} at 12–14 km height and with significant downdraughts (maximum $10\text{--}12 \text{ m s}^{-1}$) on their flanks, similar to the other studies discussed above, but they were unable to calculate the rotational field.

1.3. The present study

In this study we seek to isolate and quantify some of the basic effects of vertically oriented vorticity on deep convection in highly idealized numerical experiments.

The main calculations of M1 were carried out with a 5 km horizontal grid spacing, a little larger than that used by Hendricks *et al.* (2004) and Montgomery *et al.* (2006). One calculation was carried out with a 1.67 km grid spacing, but was not discussed in detail. All three studies were focused mainly on the collective effects of the VHTs on the system-scale vortex, although Montgomery *et al.* did examine the structure and evolution of the first VHT to develop, and they computed terms in the vorticity equation pertaining to this VHT.

The present paper is conceived as a sequel to the above studies, one of the primary goals being to isolate the effect of ambient vertical vorticity on the development of deep convection, such as when the convection develops in the environment of a tropical depression, or pre-depression circulation, or indeed, when it develops in an undisturbed tropical environment. These processes were not represented in the calculations of McCaul and Weissman (1996), where the only source of vertical vorticity was from the tilting of horizontal vorticity. Deep convection in the pre-depression environment may be markedly different from normal convection because of the presence of significant vertically oriented vorticity in the form of angular shear or horizontal shear, an expectation confirmed by the results of Rozoff referred to in section 1.1.

The calculations presented herein examine the growth of isolated deep convection in uniform environments with vertical temperature and humidity soundings typical of those in a tropical depression or pre-depression environment and in which vertical vorticity is present. One experiment, where no vertical vorticity is present, is carried out to serve as a 'control calculation'. In some cases the ambient vertical vorticity is associated with horizontal shear, in others it is associated with solid-body rotation of the background flow, or a combination of both. The calculations are highly idealized on purpose: there is no representation of boundary-layer friction and no vertical shear. As such they do not contain all the features present in realistic vortex flows, where there is both horizontal and vertical shear, and in intense vortices, where there is a potentially strong inflow jet in the boundary layer*. Nevertheless, we believe that the calculations provide a series of baseline results with which to interpret the effects of more complicated profiles possessing both vertical and horizontal shear.

The article is organized as follows. In sections 2 and 3 we give a brief description of the numerical model and the configuration of the experiments. The results are described in section 4 and the conclusions are presented in section 5.

2. The numerical model

The numerical model used for this study is the three-dimensional cloud model of Bryan and Fritsch (2002) and Bryan (2002). The model has a parametrization scheme for warm rain processes as well as one for processes involving ice microphysics. The latter is Gilmore's Li-scheme, in which cloud water, rain water, cloud ice, snow and hail/graupel are predicted (Gilmore *et al.*, 2004). The model has no parametrization of the planetary boundary

layer. For simplicity, we neglect radiation and there are no surface fluxes for momentum, heat, and moisture.

2.1. Model configuration

The horizontal domain size used for the calculations is 50 km × 50 km with a uniform horizontal grid spacing of 500 m. The vertical domain extends to a height of 28 km with the vertical grid interval stretching smoothly from 120 m at the lowest grid point up to 1 km at the top. There are 50 grid levels in the vertical, eight of which are below 850 mb. A sponge-layer is implemented in the uppermost 5 km to inhibit the reflection of gravity waves from the upper boundary. The time step is one minute and the integration time is 2 h. The default 'open' boundary conditions are used at the lateral boundaries. In the main experiments we use only the warm rain scheme, but two experiments are carried out to investigate the additional effects of ice microphysics.

2.2. Environmental sounding

As a first attempt to represent ambient conditions similar to those in the inner region of an incipient tropical depression, we take the temperature and humidity profiles from a time average of those obtained from the seven Barbados radiosonde soundings for the period 0000 UTC on 9 September 2010 to 0000 UTC on 12 September 2010. This period overlapped the passage of the tropical depression that eventually developed into hurricane *Karl*. The temperature and dew-point temperature are shown in a skew T -log p diagram in Figure 1. The sounding has a total precipitable water of 52.5 kg m⁻² and a CAPE of about 1.8 kJ kg⁻¹.

2.3. Representation of vertical vorticity

In the majority of the calculations, the value of the vertical vorticity is taken to be $\zeta_o = 3 \times 10^{-4} \text{ s}^{-1}$. This value is approximately equal to that at low levels in the initial

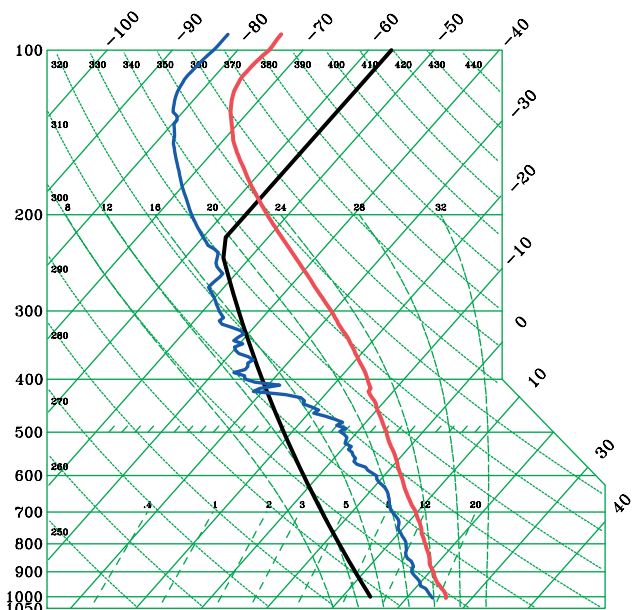


Figure 1. Skew T -log p diagram showing the temperature and dew point temperature of the initial sounding. The bold solid curve is the standard-atmosphere sounding. This figure is available in colour online at wileyonlinelibrary.com/journal/qj

* A recent discussion of the dynamical role of the boundary layer on tropical cyclone intensification is given by Smith *et al.* (2009) and also Smith and Montgomery (2011).

Table I. Details of the nine experiments studied.

Experiment	Microphysics	Horizontal shear	f	ΔT (K) ^a	Modified OW ^b
1	warm rain	none	none	3.5	0
2	warm rain	ζ_o	none	3.5	0
3	warm rain	$0.5 \zeta_o$	$0.5 \zeta_o$	3.5	$0.75 \zeta_o^2$
4	warm rain	none	ζ_o	3.5	ζ_o^2
5	warm rain	$2\zeta_o$	none	3.5	0
6	warm rain	none	$5 \times 10^{-5} \text{ s}^{-1}$	3.5	$2.5 \times 10^{-11} \text{ s}^{-1}$
7	warm rain	none	$5 \times 10^{-5} \text{ s}^{-1}$	2.6	$2.5 \times 10^{-11} \text{ s}^{-1}$
8	rain + ice	ζ_o	none	3.5	0
9	rain + ice	none	ζ_o	3.5	ζ_o^2

ζ_o has the value $3 \times 10^{-4} \text{ s}^{-1}$.

^a The strength of the initial thermal perturbation.

^b The modified Okubo–Weiss parameter discussed in the text.

vortex of the control experiment in M1, also at a radius of 90 km, but here, for simplicity, the vorticity does not vary with height. We consider two extreme situations and an intermediate situation as follows. In the first extreme, the vertical component of relative vorticity is entirely shear vorticity associated with a background flow with uniform horizontal shear over the whole domain. Specifically, we take the wind in the meridional (y) direction to given by:

$$v(x) = \frac{V_s}{d} \left(x - \frac{d}{2} \right), \quad (1)$$

where V_s is the wind difference across the domain, x is the zonal coordinate along the middle of the domain, and $d = 50 \text{ km}$ is the width of the domain. This flow has a uniform vertical component of relative vorticity, $\zeta_o = V_s/d$. In the second extreme we consider an environment of uniform rotation about a vertical axis $f/2$, where $f = \zeta_o$. The intermediate situation has uniform background rotation $0.25 \zeta_o$ ($f = 0.5 \zeta_o$) and uniform shear with vertical vorticity $V_s/2d = 0.5 \zeta_o$.

We have not sought to initialize the calculations from a geostrophically balanced state, partly because the Bryan model is not easily configured to allow this, but also because we are interested in times much shorter than the inertial period (on the order of 6 h). This omission did not appear to have any adverse effects at the horizontal boundaries.

2.4. Initiation of convection

Convection is initiated using a symmetric thermal perturbation with a horizontal radius of 10 km, a vertical extent of 2 km, and a maximum temperature excess of 3.5 K at a height of 1 km (in one experiment the temperature excess was reduced to 2.6 K). The temperature excess is a maximum at the centre of the perturbation and decreases gradually to 0 K at its edge. While this method for the initiation of convection is artificial, it has been widely used in numerical studies of deep convection (e.g. Weisman and Klemp, 1982; Gilmore *et al.*, 2004; Rozoff, 2007; Wissmeier, 2009[†]). Of course, the details of the ensuing convection may be expected to depend on the spatial structure of the

thermal perturbation and, as shown later, the depth of the ensuing convection depends on the amplitude of the initial perturbation. Nevertheless, it is reasonable to assume that the differences between the convection that evolves in different configurations of vertical vorticity starting with the same thermal perturbation will reflect the differences that would occur with another, possibly more realistic, triggering mechanism. Moreover, the precise way in which the convection is initiated is of little consequence for the mechanism that we want to isolate in this article.

3. The numerical experiments

Table I shows a list of the nine experiments studied and their respective parameter values. Experiment 1 is a calculation for a quiescent environment with no background vorticity. This experiment serves as a control experiment with which to compare the other experiments that all have non-zero vertical vorticity. Experiments 2–4 have initially the same uniform distribution of vertical vorticity, $\zeta_o = 3 \times 10^{-4} \text{ s}^{-1}$. In Experiment 2, all the vorticity lies in the shear and there is no background rotation. In Experiment 4, the calculation is performed on an f -plane with the same value of vertical vorticity as in Experiment 2. Experiment 3 corresponds with the intermediate situation described in section 2.3. It is carried out on an f -plane with half the angular rotation of Experiment 4 and has half the horizontal shear of Experiment 2. Experiment 5 is similar to Experiment 2, but has twice the value of horizontal shear, i.e. $V_s/d = 2\zeta_o$.

Rozoff *et al.* (2006) have argued that an important parameter relevant to delineating regions of a tropical cyclone favourable to deep convection from those that are unfavourable is the Okubo–Weiss parameter (OW) defined as:

$$OW = \zeta^2 - E^2 - F^2, \quad (2)$$

where $\zeta = \partial v/\partial x - \partial u/\partial y$ is the vertical component of relative vorticity and E and F are the stretching and shearing components of the deformation field. The latter are defined by $E = \partial u/\partial x - \partial v/\partial y$ and $F = \partial v/\partial x + \partial u/\partial y$, where u and v are the horizontal velocity components in the rectangular coordinate system (x, y) . Thus the magnitude and sign of OW provide a measure of the relative importance of the local rotation to local strain, with the rotation-dominated regime having positive values

[†]Section 3.4.2 therein examines the sensitivity of the storm's initial updraught strength on the warm bubble parameters (width, depth, temperature excess).

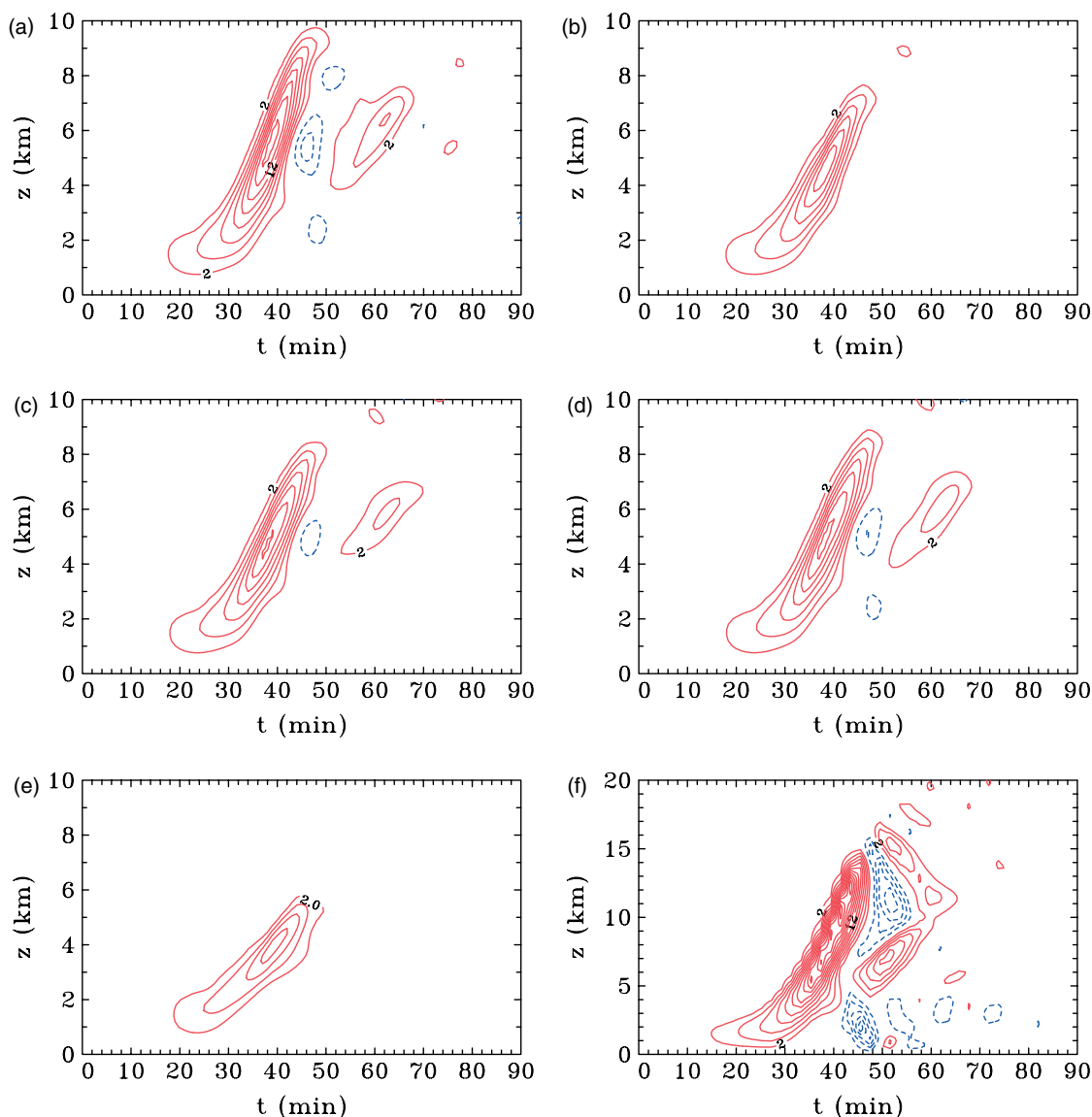


Figure 2. Height-time cross sections of maximum vertical velocity taken at the centre of the hot tower in Experiments 1–5 and 9: (a) Experiment 1, (b) Experiment 2, (c) Experiment 3, (d) Experiment 4, (e) Experiment 5, and (f) Experiment 9. (Details of the experiments are given in Table I.) The contour interval is 2 m s^{-1} with solid contours showing positive values, and dashed contours negative values. Note the different scale on the ordinate in (f). This figure is available in colour online at wileyonlinelibrary.com/journal/qj

and the strain-dominated regime having negative values. We argue that a relevant extension of OW to the present experiments would be to replace the relative vorticity by the absolute vorticity, $\zeta + f$, because, in these experiments, the stabilizing effects of rotation reside in the background rotation. Then Experiments 2–5 span the range of values of this modified OW from zero in Experiment 2, $0.75 \zeta_o^2$ in Experiment 3, ζ_o^2 in Experiment 4 and again zero in Experiment 5. Values of OW for the various experiments are listed also in Table I.

The expectation from Rozoff *et al.* (2006) is that negative values of the parameter (i.e. relatively high strain) are especially detrimental to deep convection, while substantially positive values are favourable. While the simple experiments described here are able to cover only non-negative values of OW , it is found that even a zero value of OW is detrimental to the convection. However, we will show that OW is not the sole parameter governing the strength of convection: the magnitude of the shear is of overriding importance.

Experiment 6 is a repeat of Experiment 4, but with a nominal tropical value of f ($5 \times 10^{-5} \text{ s}^{-1}$), while Experiment 7 is a repeat of Experiment 6, but with the strength of the initial thermal perturbation reduced to 2.6 K. These experiments are carried out to quantify the degree of amplification of the background rotation by deep convection in an environment typical of the undisturbed tropical atmosphere and by shallower, cumulus congestus clouds.

Experiments 8 and 9 are repeats of Experiments 2 and 4, but include a representation of ice microphysics as described in section 2. There is no ambient vertical shear in any of the experiments.

4. Results

Much of our interest herein is focused on the life cycle of the first convective updraught cell to develop in response to the initial thermal bubble, i.e. the first hour of the simulation. In fact, in all experiments except those including

ice microphysics, subsequent cells do not occur for the sounding used here.

4.1. Convective cell evolution

The evolution of the updraught in Experiments 1–5 and Experiment 9 is summarized in Figure 2 by time-height cross-sections of vertical velocity at the centre of the domain where the updraught forms. To begin, we focus on the first five warm rain calculations. Experiments 6 and 7 will be discussed in section 4.6 and Experiments 8 and 9 in section 4.7.

Figures 3 and 4 show the corresponding cross-sections of total liquid water (cloud water plus rainwater) and the density temperature[‡] difference, dT_ρ , between the updraught and the environment for Experiments 2 and 4. The quantity dT_ρ characterizes the buoyancy of the updraught. The patterns of these two fields in the other experiments are broadly similar.

In all experiments, the evolution is similar to that which has been described many times previously[§], so we give only a brief description. The updraught that forms the first convective cell is initiated by the buoyancy of the initial bubble. The updraught develops slowly at first, but increases rapidly in vertical extent and strength as additional buoyancy is generated by the latent heat release of condensation. The cloud water produced by condensation is carried aloft in the updraught and the rain water that develops falls to the ground. In the warm rain experiments, the maximum vertical velocity is attained in the middle troposphere after about 36–40 min, but with the inclusion of ice microphysics it occurs in the upper troposphere. Thereafter, the updraught decays as a result of water loading and a downdraught forms. The downdraught is cooled by the partial evaporation of rain as it falls into unsaturated air below cloud base and a cold pool forms near the surface. For the chosen sounding, the associated cold-air outflow triggers mostly gravity waves as the sounding is too stable and the downdraughts too weak to allow the formation of further cells. However, with more unstable soundings, the spreading gust triggers secondary cells and the subsequent flow evolution becomes more complicated than that shown here. A more detailed study of such cases is in progress and the results will be reported in due course.

The downdraughts in the warm rain experiments tend not to exceed 5 m s^{-1} (Table II), but they are much stronger when ice processes are included (between 10 and 12 m s^{-1}), presumably because of melting below the freezing level (e.g. Figure 2(f)). The small regions of alternate positive and negative vertical velocity above about 15 km in Figure 2(f) are signatures of internal gravity waves initiated by the convection that propagate upwards into the stratosphere.

4.2. The effects of ambient vertical vorticity

Details of the updraught strength, the maximum density temperature difference between the updraught and

the environment ($dT_{\rho \text{ max}}$), the maximum liquid water content, and the maximum vertical vorticity are given in Table II. In the first five experiments, the strongest updraught (17 m s^{-1}) occurs in Experiment 1, where there is no vertical vorticity, and the second strongest (15 m s^{-1}) when there is vertical vorticity, but no horizontal shear (Experiment 4). These maximum updraught strengths are weaker than those reported by Houze *et al.* (2009) and Guimond *et al.* (2010), but note that these five experiments have no representation of ice microphysics. When the latter are included, the maximum updraught strengths are comparable to those observed.

Horizontal shear leads to greater entrainment into the updraught as evidenced by a reduction of the cloud buoyancy and liquid water content of the updraught. As expected, there is a monotonic relationship between the maximum vertical velocity and the maximum buoyancy, as characterized by $dT_{\rho \text{ max}}$, and the maximum liquid water content (Table II). In particular, there is a clear decrease in the buoyancy and water loading as the horizontal shear increases.

In all except Experiment 1, the developing updraught stretches the ambient relative vorticity, leading to a significant amplification of the vorticity as discussed below. It is this feature that is of primary interest in this article. In the suite of calculations reported here, *the updraught is weakened by the presence of ambient vertical vorticity* (Table II and compare the first four panels of Figure 2). We discuss the reasons for this weakening in section 4.5.

The dependence of updraught intensity on the shear found above is consistent with the reasoning of Rozoff *et al.* (2006) that the convection will be weakened as the fraction of shear to curvature vorticity increases, i.e. as OW becomes smaller. However, the fact that the updraught is much weaker in Experiment 5 than in Experiment 2 suggests that the strength of the shear is the more important parameter affecting the strength of convection, since OW is zero in both of these experiments.

A most striking feature of Experiments 2–5 is the exceedingly large amplification of the vertical component of relative vorticity at low levels. In Experiments 2–4, the maximum vorticity is about 25 times that of the background vorticity (Table II and compare Figures 5(a–c)). Apparently, vertical vorticity in the form of horizontal shear is not detrimental to reducing the degree of amplification of the vorticity as it is in reducing the strength of the updraught. Indeed, reducing the proportion of shear vorticity keeping the total vorticity the same does not effectively change the degree of amplification. Doubling the magnitude of the horizontal shear present in Experiment 2 leads to a marginally weaker vertical vorticity (compare Figures 5(a, d) and see Table II) and the amplification is 12 times the initial ambient value ($2\zeta_0$ in this case).

The maximum values of vorticity in Table II corroborate the recent observational estimates of Houze *et al.* (2009), Bell and Montgomery (2010) and Raymond and López-Carillo (2011), who found local values in regions of deep convection well over an order of magnitude larger than the areal average values of vorticity in the central region of developing depressions and typically exceeding 10^{-3} s^{-1} .

[‡]The density temperature, $T_\rho = T(1 + r/\alpha)/(1 + r_t)$, where T is the absolute temperature, r is the mixing ratio for water vapour, r_t is the mixing ratio of total water substance and α is the ratio of the specific gas constants for liquid water and dry air (e.g. Emanuel, 1994, p 113). Outside clouds it is equal to the virtual temperature.

[§]A good example is Rozoff (2007) Figure 4.4, and the discussion thereof.

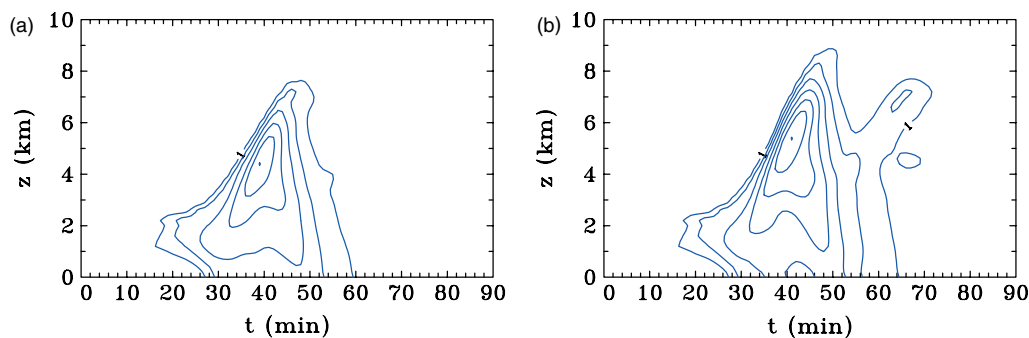


Figure 3. Height-time cross sections of maximum total liquid water (cloud water + rain water) taken at the centre of the hot tower in (a) Experiment 2, and (b) Experiment 4. The contour interval is 1 g kg^{-1} . This figure is available in colour online at wileyonlinelibrary.com/journal/qj

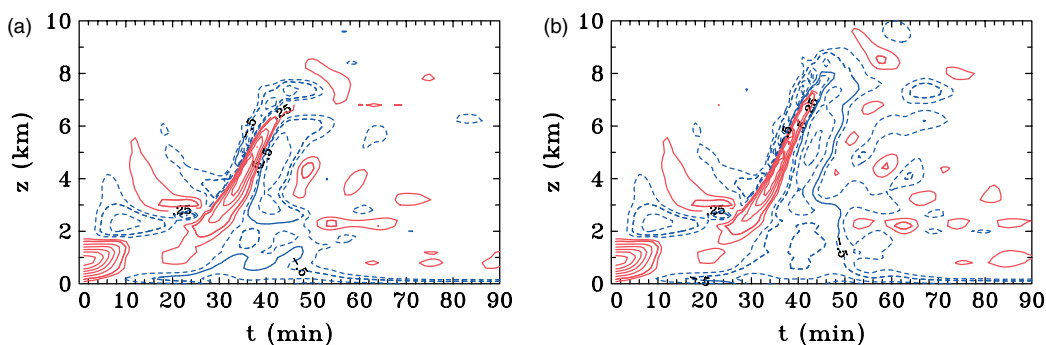


Figure 4. Height-time cross sections of maximum buoyancy, characterized by the density temperature of the centre of the updraught minus the virtual temperature of the environment in Experiments 2 and 4. The contour intervals are 0.5 K . The thin curves show the $\pm 0.25 \text{ K}$ contours. The solid contours show positive values, and dashed contours negative values. The small regions of alternate positive and negative buoyancy above about 8 km , especially prominent in (b), are signatures of upward-propagating internal gravity waves initiated by the convection. This figure is available in colour online at wileyonlinelibrary.com/journal/qj

4.3. Persistence of enhanced vertical vorticity

A significant result of the foregoing simulations is that the region of enhanced vorticity remains long after the updraught and associated precipitation field have decayed. In a tropical cyclone, this vorticity would be available to interact with like-signed patches produced by neighbouring convective cells, to be strengthened further by subsequent

convection, and to be progressively axisymmetrized by the angular shear of the parent vortex as discussed by Hendricks *et al.* (2004), Montgomery *et al.* (2006) and in M1.

4.4. Horizontal and vertical structure of cells

Figure 6 shows horizontal cross-sections of vertical velocity at a height of 2 and 5 km for Experiments 2 and 4 at selected

Table II. Results from Experiments 1–9. Here, $\zeta_1 = \zeta_0$ in all except Experiment 5, where it is equal to $2\zeta_0$, and Experiments 6 and 7, where it is $5 \times 10^{-5} \text{ s}^{-1}$. In Experiments 5 and 7, w_{\min} is associated with a gravity wave induced by a collapsing updraught rather than with a precipitation-cooled downdraught.

Experiment	w_{\max} (m s^{-1})	$z(w_{\max})$ (km)	w_{\min} (m s^{-1})	$z(w_{\min})$ (km)	$q_{L \max}$ (g kg^{-1})	ζ_{\max}/ζ_1	$t_{\zeta_{\max}}$ (min)	$dT_{\rho \max}$ (K)	$z(dT_{\rho \max})$ (km)
1	17	5.8	-4.9	5.4	8.4	0	–	2.7	4.4
2	13	4.8	-2.0	1.8	6.0	25	81	2.5	4.2
3	14	4.8	-3.3	5.0	6.5	26	89	2.4	4.2
4	15	4.8	-4.1	5.2	7.0	25	81	2.5	4.2
5	9	4.0	-1.3	1.8	3.4	12	59	1.6	3.6
6	17	5.6	-4.8	5.4	8.4	67	90	2.7	4.4
7	6	3.0	-1.8	2.8	2.6	21	90	0.7	2.4
8	23	10.0	-10.4	1.6	12.1	24	27	3.6	6.4
9	25	10.6	-11.6	2.0	13.8	32	27	3.7	6.4

w_{\max} is the maximum vertical velocity at the centre of the domain, and $z(w_{\max})$ the height of this maximum, w_{\min} is the minimum vertical velocity below 10 km at the domain centre, and $z(w_{\min})$ the height of this minimum, $q_{L \max}$ is the maximum liquid water content, ζ_{\max}/ζ_1 is the degree of amplification of the ambient vorticity, and $t_{\zeta_{\max}}$ the time at which it occurs in Exps 2–9. $dT_{\rho \max}$ is the maximum density temperature difference between the updraught and the environment, and $z(dT_{\rho \max})$ the height at which this maximum occurs.

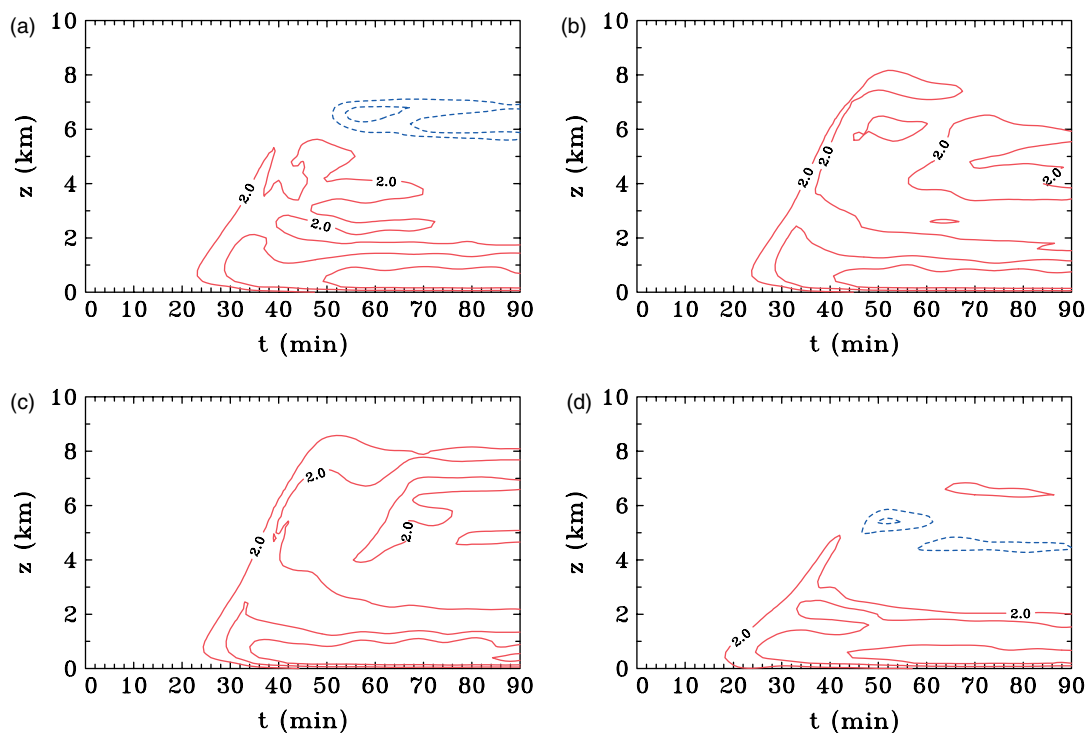


Figure 5. Height-time cross sections of maximum vertical component of relative vorticity taken in the centre of the updraught in Experiments 2–5: (a) Experiment 2 with horizontal shear $\zeta_0 = 3 \times 10^{-4} \text{ s}^{-1}$ and no background rotation; (b) Experiment 3 with horizontal shear $0.5 \zeta_0$ and uniform background rotation with $f = 0.5 \zeta_0$; (c) Experiment 4 with no horizontal shear, but uniform background rotation with $f = \zeta_0$; (d) Experiment 5 with horizontal shear $2 \zeta_0$ and no background rotation. The contour interval is $2 \times 10^{-3} \text{ s}^{-1}$. The solid contours show positive values, dashed contours negative values. This figure is available in colour online at wileyonlinelibrary.com/journal/qj

times, while Figure 7 shows similar cross-sections of relative vorticity at a height of 500 m. In both experiments, the updraught peaks in strength after 38–39 min. At 40 min the updraught at 5 km in Experiment 2 is slightly elongated in the meridional direction, as is the corresponding relative vorticity structure, an asymmetry that is clearly associated with the horizontal shear because it does not occur[†] in Experiment 4.

The rapid collapse of the updraught leads to the generation of a gravity wave, which is most evident in the vertical motion fields at 50 min. In Experiment 2, these waves have an azimuthal wavenumber-2 pattern on account of the horizontal shear, while in Experiment 4 they are essentially axisymmetric. With more convectively unstable soundings, the gravity waves lead to the formation of a pair of secondary updraughts (not shown), similar to those described by Rozoff (2007). Rozoff showed the morphology of the total liquid water field for such a sounding over a 96 min integration from the initial state (his Figure 4.11).

The foregoing structures are a little different from those shown by Montgomery *et al.* (2006), who found more of a dipole structure in the vorticity field, albeit with the cyclonic gyre significantly stronger than the anticyclonic gyre. The reason for these differences is the presence also of low-level vertical shear in their calculations, an effect that is absent in the present ones. Nevertheless the degree of amplification of the ambient vertical vorticity in their calculations is similar to that in ours. We plan to examine the additional effects of vertical shear in a forthcoming article.

[†]The departures from purely axisymmetric fields in (c) and (d) of both Figures 6 and 7 are a result of the relatively coarse resolution of the features being plotted.

Figure 8(a) shows the vertical structure of the tangential wind speed through the centre of the convective cell at 40 min in Experiment 4, just after the vertical velocity has peaked. At this time, the maximum tangential wind speed is a little over 2.5 m s^{-1} and occurs at an altitude of about 1 km and a radius of about 500 m (although recall that this radius is just the horizontal grid spacing). After 90 min (Figure 8(b)), the tangential wind maximum is slightly larger, about 3 m s^{-1} . The question that immediately arises is whether these induced tangential winds are large enough to have a measurable effect on the radial force balance? We examine this question in the next subsection.

4.5. Force balance in the updraught

Figures 8(c) and (d) show height-radius distributions of the radial pressure gradient in Experiment 4 at 40 and 90 min respectively, and (e) and (f) show the corresponding distributions of the agradiant force. The agradiant force is the sum of the radial pressure gradient force per unit mass and the centrifugal and Coriolis forces associated with the tangential wind distribution, shown in (a) and (b). At each time, the radial pressure gradient and agradiant force fields are mostly similar, suggesting that the centrifugal and Coriolis forces do not play a strong role in the dynamics of the updraughts. The exception at 40 min is the region below an altitude of 2 km where the inward-directed radial pressure-gradient force (Figure 8(c)) is clearly reduced by the centrifugal and Coriolis forces, i.e. the agradiant force in Figure 8(e) is reduced in this region. Simple adjustment considerations would suggest that the flow would tend towards a balanced state on a time-scale that is inversely proportional to the local vorticity, but the situation here

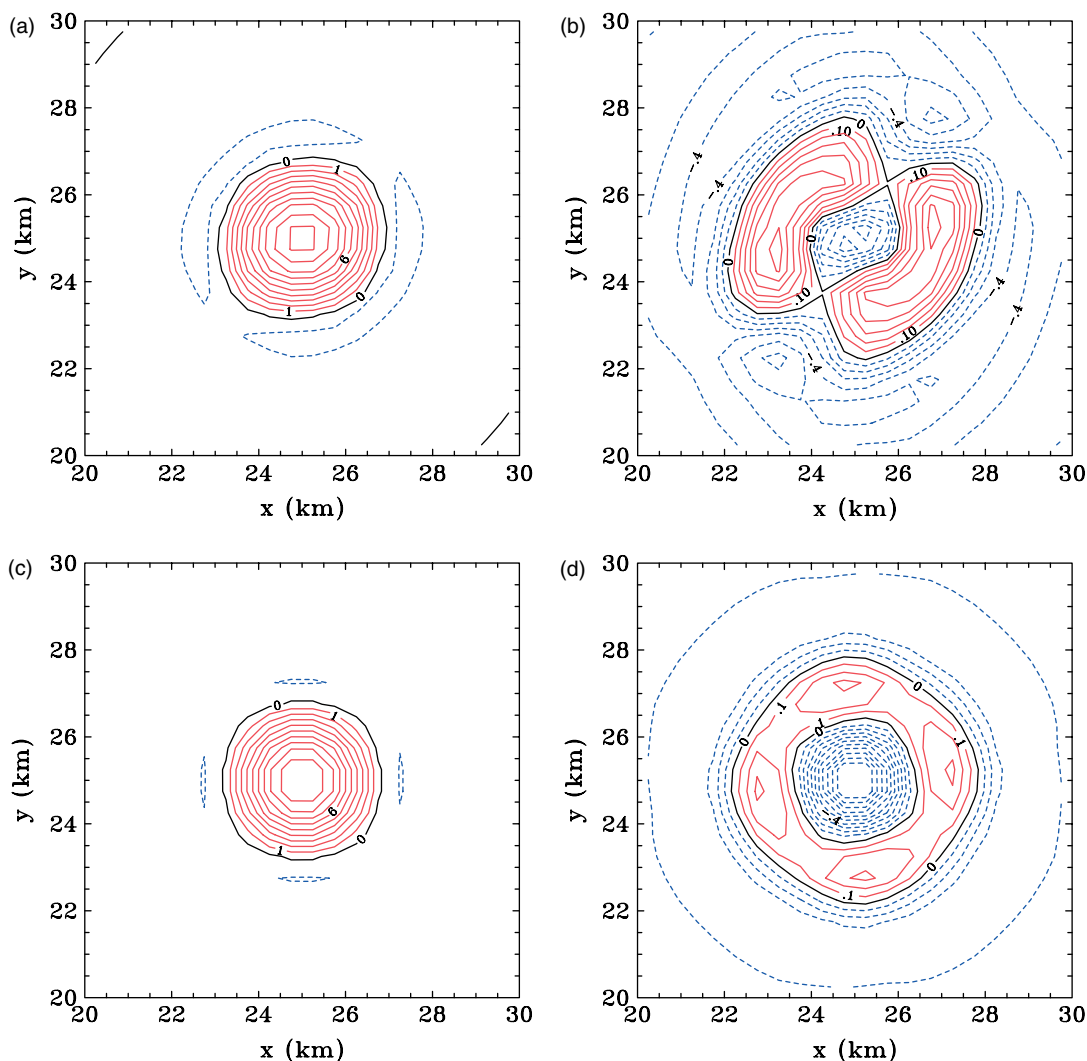


Figure 6. Horizontal cross-sections of vertical velocity in (a, b) Experiment 2 and (c, d) Experiment 4 at (a, c) 40 min and a height of 5 km, and (b, d) 50 min and a height of 2 km. The contour intervals are 1 m s^{-1} (thick contours) and 0.1 m s^{-1} (thin contours), with solid contours showing positive values, and dashed contours negative values. The departures from purely axisymmetric fields in (c) and (d) are a result of the relatively coarse resolution of the features being plotted. This figure is available in colour online at wileyonlinelibrary.com/journal/qj

is complicated by the transient nature of the flow on this time-scale. Even after 90 min, the low-level vortex is not in close gradient wind balance: comparing Figures 8(f) and (d) shows that, at this time, the agradient force is outwards, while the radial pressure gradient is inwards. It should be recalled that frictional effects, which are not considered in these calculations, would reduce the centrifugal and Coriolis forces at low levels, possibly resulting in an inward agradient force there.

The foregoing results do not support the general statement in Montgomery *et al.* (2006) that ‘the intense cyclonic vorticity cores possess an intrinsic centrifugal and vortex-Rossby elasticity that tends to protect them from detrimental effects of lateral entrainment’. Whether or not this statement is valid as the background vorticity increases remains to be determined. It is conceivable that, at later stages of the evolution of a vortex, after a number of convectively induced patches of vorticity have amalgamated, the VHTs may have a greater degree of elasticity. An investigation of this possibility will be a topic for future research.

It is seen from Figure 8 that the centrifugal and Coriolis forces oppose the radial pressure gradients driving inflow

into the updraught below about 6 km. This fact explains why the updraught strength is reduced in the cases with non-zero vertical vorticity, since any resistance to inflow will reduce the strength of the updraught through continuity considerations. The continuity constraint requires a commensurate reduction in the vertical perturbation pressure gradient (e.g. Smith *et al.*, 2005, section 7).

We have not performed similar agradient-force calculations for Experiments 2, 3 and 5 because the flow in these is not axisymmetric. In these experiments the situation is more complicated because one would have to calculate the agradient force relative to an axisymmetric mean state centred on the updraught and the force would be a function also of azimuth.

4.6. Convection in environments of weaker ambient rotation

Hitherto, the importance of ambient vertical rotation on deep convection has been emphasized in connection with tropical depressions or tropical storms, but the fluid-dynamical nature of vortex-tube stretching by convective updraughts is a fundamental process independent of the strength of the ambient vorticity. Indeed, the mechanism

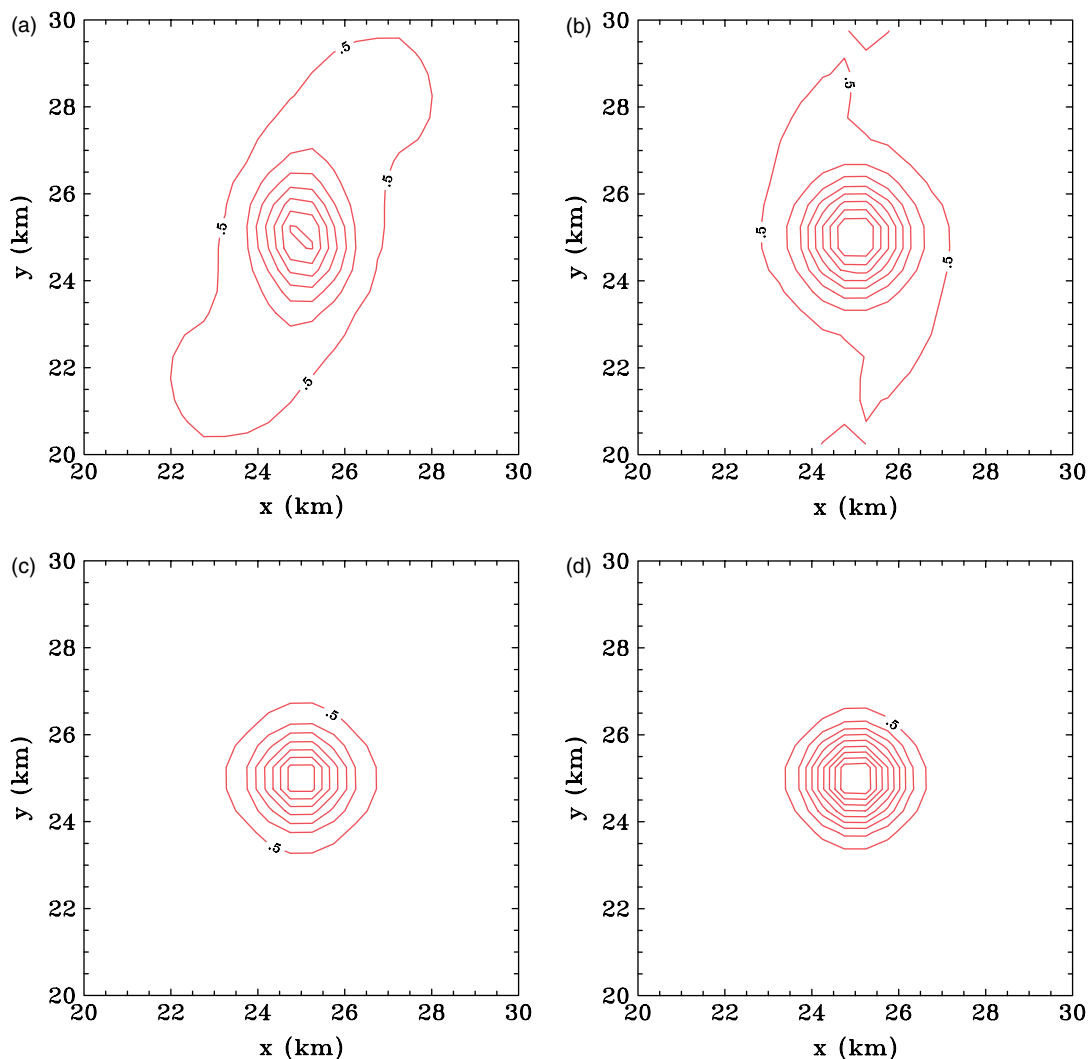


Figure 7. Horizontal cross-sections of relative vorticity at a height of 500 m in (a, b) Experiment 2 and (c, d) Experiment 4 at (a, c) 40 min and (b, d) 90 min. The contour interval is $5 \times 10^{-4} \text{ s}^{-1}$. The departures from purely axisymmetric fields in (c) and (d) are a result of the relatively coarse resolution of the features being plotted. This figure is available in colour online at wileyonlinelibrary.com/journal/qj

should operate even in the undisturbed tropical atmosphere and the question arises as to how much amplification of the rotation can be achieved at such low values of ambient rotation. We address this question here by carrying out Experiments 6 and 7, which are similar to Experiment 4, but where the Coriolis parameter is set to $5 \times 10^{-5} \text{ s}^{-1}$, typical of the undisturbed tropical atmosphere. Experiment 6 is otherwise the same as Experiment 4, but in Experiment 7, the amplitude of the initial thermal perturbation is reduced to 2.6 K so that the ensuing convection is shallower, more akin to a cumulus congestus cloud. The pertinent results are summarized in Figure 9, which shows height-time series of maximum vertical component of relative vorticity taken in the centre of the updraught in these two experiments. Details of these experiments are included in Table II.

It is evident that, even for a background rotation rate typical of the undisturbed tropical atmosphere, and even for updraughts of only moderate vertical extent such as those of cumulus congestus clouds, the convection produces a significant amplification of the low-level vertical vorticity. In fact, the amplification is nearly three times that in Experiments 2–4. Of course, the associated tangential winds are tiny (with maxima on the order of 1 m s^{-1})

and would be barely measurable. We believe that this finding has important implications for our understanding of tropical cyclogenesis. Indeed, it provides a basis for a unified theory of tropical cyclogenesis and tropical cyclone intensification as suggested in a recent review article on tropical cyclone formation by Montgomery and Smith (2010).

4.7. Inclusion of ice microphysics

The principal effect of the inclusion of ice microphysics is to increase the updraught buoyancy, which, of course, leads to a stronger updraught (Table II and Figure 2(f)). In Experiment 8, the maximum vertical velocity is 23 m s^{-1} , compared with 13 m s^{-1} in Experiment 2, and in Experiment 9 the maximum is 25 m s^{-1} , compared with 15 m s^{-1} in Experiment 4. The maximum vertical velocities attained with ice microphysics are in the range of those so far reported from the observational studies, but they are a little less than those found in the model calculations of Montgomery *et al.* (2006) and Rozoff (2007), presumably because the sounding we use is more stable.

Figure 10 shows time-height cross-sections of the maximum vertical component of relative vorticity taken

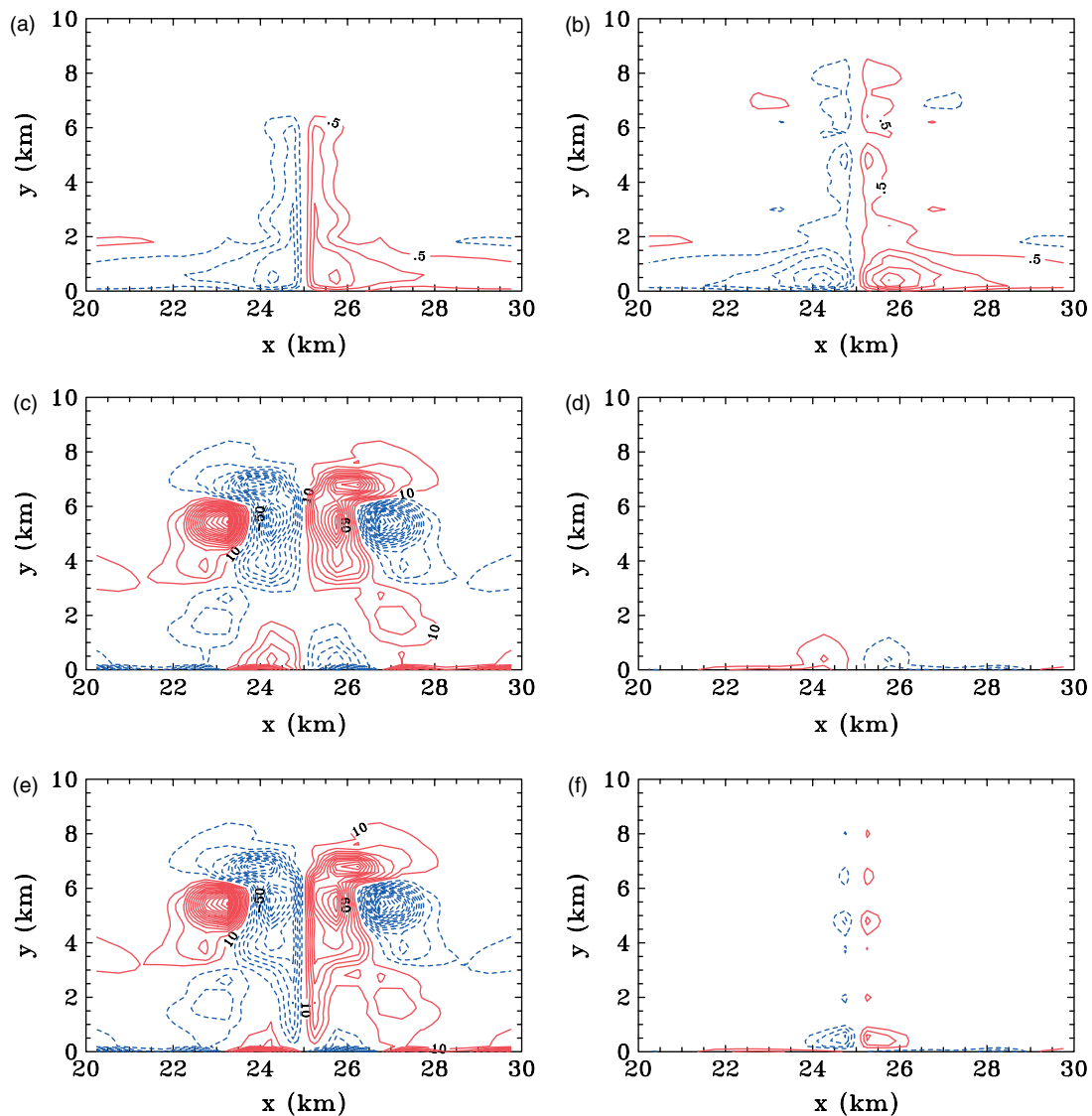


Figure 8. Zonal-height cross-sections along the centre of the domain of: (a, b) tangential velocity, (c, d) radial pressure gradient, and (e, f) gradient force in Experiment 4 at (a, c, e) 40 min and (b, d, f) 90 min. The contour interval for tangential wind is 0.5 m s^{-1} and for the force fields is 10 m s^{-1} per hour. Solid contours denote positive values, and dashed contours negative. This figure is available in colour online at wileyonlinelibrary.com/journal/qj

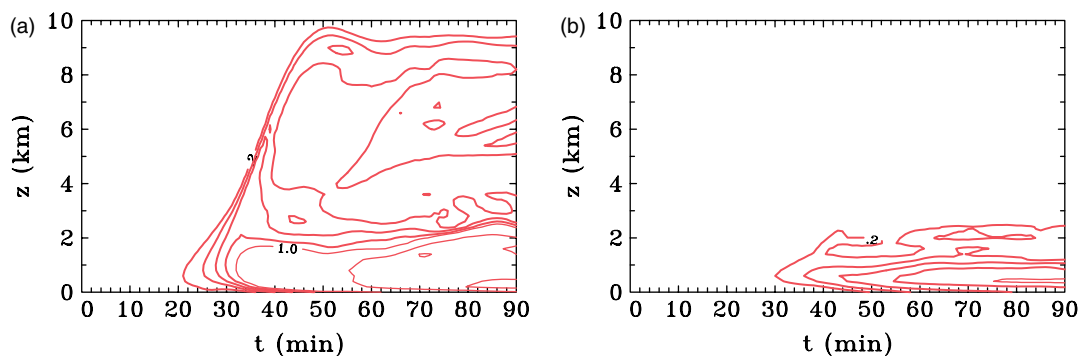


Figure 9. Height-time cross sections of the maximum vertical component of relative vorticity taken in the centre of the updraught in (a) Experiment 6, and (b) Experiment 7. The contour intervals are $1 \times 10^{-3} \text{ s}^{-1}$ (thick curves), and $2 \times 10^{-4} \text{ s}^{-1}$ (thin curves). This figure is available in colour online at wileyonlinelibrary.com/journal/qj

in the centre of the updraught in Experiments 8 and 9. Interestingly, the increases in vertical velocity with the inclusion of ice microphysical processes are not reflected in commensurate increases in the low-level relative vorticity, presumably because the additional vertical stretching associated with the stronger updraught is largest at upper

levels and because of the stronger downdraughts when ice is present (e.g. Figure 2(f)). The stronger downdraughts would lead to stronger low-level divergence that would act to reduce the vorticity at the lowest levels, but they will contribute to additional stretching of vertical vorticity at higher levels where the air converges to feed the updraught

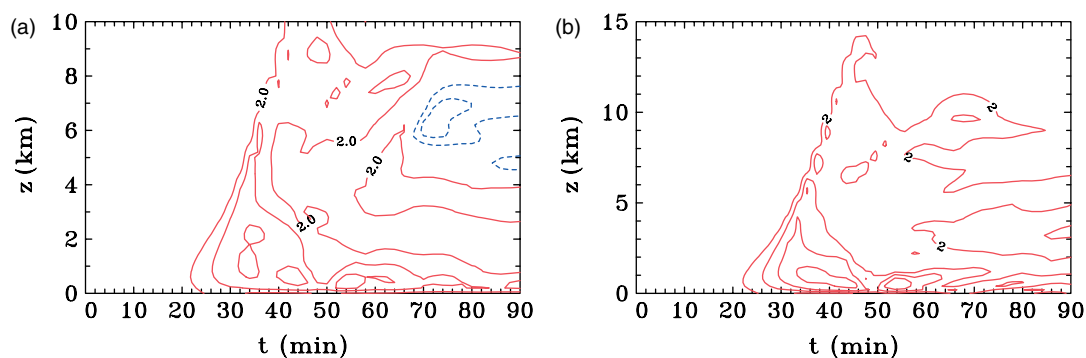


Figure 10. As Figure 9, but for (a) Experiment 8, and (b) Experiment 9, both of which have a representation of ice microphysics. The contour interval is $2 \times 10^{-3} \text{ s}^{-1}$. This figure is available in colour online at wileyonlinelibrary.com/journal/qj

above. The maximum tangential wind speed in Experiment 9 after 90 min is 2.3 m s^{-1} , which is fractionally less than that in Experiment 4 (3.0 m s^{-1}), showing that it is not only the deep clouds that produce a significant amplification of the background rotation. Obviously what matters is a rapid vertical acceleration in the lower troposphere that would be favoured by large low-level parcel buoyancy in the sounding.

4.8. Vertical mass flux

In section 4.1 we discussed, *inter alia*, the evolution of the vertical velocity in several of the experiments and used this quantity as a measure of the updraught strength. However, it is the vertical mass flux ρw that appears in the stretching term of the vertical vorticity equation for a compressible atmosphere, where w is the vertical velocity and ρ the density. Indeed, the vorticity tendency due to stretching is $(1/\rho)\partial(\rho w)/\partial z$. Because ρ decreases approximately exponentially with height, we expect the vertical profile of mass flux to have a lower maximum than that of the vertical velocity itself. As an illustration of the differences between the vertical velocity and vertical mass flux, we show in Figure 11 the height-time behaviour of the mass flux along the axis in Experiment 9, which should be compared with Figure 2(f). Note that the maximum mass flux occurs at a height of 5.5 km, compared with 10.6 km for the vertical velocity. Changes in height of the level of the mass flux maximum have been invoked as being important during tropical cyclogenesis (Raymond and Sessions, 2007).

5. Conclusions

We have presented a series of numerical experiments designed to isolate the effects of ambient vertical vorticity on the development of deep convection, the main focus being on convection that develops within tropical depressions and pre-depressions. The vertical vorticity is represented by a uniform horizontal shear or uniform solid-body rotation or a combination of both.

In the experiments described, the presence of ambient vertical vorticity reduces the updraught strength, slightly more so when the vorticity is associated with horizontal shear than when it is associated with solid-body rotation. The dependence of updraught intensity on the shear described herein supports the reasoning of Rozoff *et al.* (2006) that deep convection will be weakened as the fraction of shear

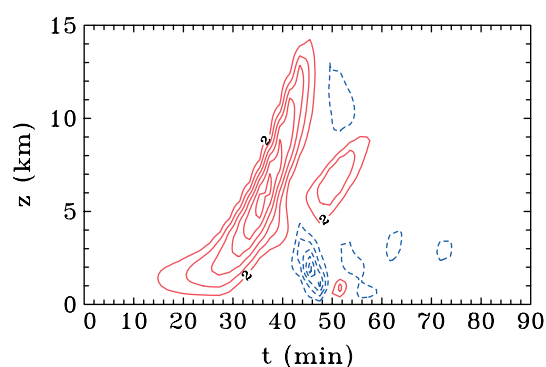


Figure 11. Height-time series of the vertical mass taken in the centre of the updraught in Experiment 9. The contour interval is $2 \text{ kg m}^{-2} \text{ s}^{-1}$, with solid contours denoting positive values, and dashed contours negative. This figure is available in colour online at wileyonlinelibrary.com/journal/qj

to curvature vorticity increases, i.e. as the Okubo–Weiss parameter becomes smaller or negative. We attribute the reduction of updraught strength to the reduction of the radial inflow by the centrifugal and Coriolis forces as a result of the continuity constraint and, in the presence of horizontal shear, to a reduction of cloud buoyancy brought about by entrainment. Our experiments with uniform horizontal shear are able to span only non-negative values of the (modified) Okubo–Weiss parameter. In the two experiments where the parameter is zero (no background rotation, uniform horizontal shear), we found that the larger shear was more detrimental to the convection, indicating that the value of the (modified) Okubo–Weiss parameter is not the sole parameter in determining the inhibition of convection by horizontal strain.

We have shown that the low-level vorticity stretching by growing convective cells amplifies the ambient rotation at low levels by more than an order of magnitude, and that the vorticity produced persists long after the initial updraught has decayed. The predicted vorticity values are comparable with those reported in recent observational studies of tropical depressions. Despite the significant amplification of vorticity, the sum of the centrifugal and Coriolis forces is mostly small compared with the radial pressure gradient force, so that the induced rotation does not have a large effect on the updraught dynamics. Thus, at the level of background rotation studied, the previously postulated effects of Rossby elasticity appear to be unimportant. In order for these effects to be important, the convection would need to persist for a longer time or the levels of background rotation would need to be larger.

We have shown that significant amplification of the vertical vorticity occurs even for a background rotation rate typical of the undisturbed tropical atmosphere and even for clouds of only moderate vertical extent such as cumulus congestus clouds. We consider this finding to have important implications for tropical cyclogenesis, providing a basis for a unified theory of tropical cyclogenesis and tropical cyclone intensification as discussed in a recent review paper by Montgomery and Smith (2010).

These highly-idealized simulations ignore several processes that are likely to be important in reality, such as ambient vertical shear and surface friction. Nevertheless, they provide benchmark calculations for interpreting more complex situations that may include such effects. Calculations designed to investigate these additional complexities are under way together with calculations to isolate the processes involved in the interaction of two initial cells.

Acknowledgements

We are grateful to Michael Montgomery for his stimulating and perceptive comments on an earlier draft of this manuscript. We thank also Chris Rozoff, Sarah Jones and an anonymous reviewer for their careful and penetrating reviews. This research was supported by the German Research Council (Deutsche Forschungsgemeinschaft).

References

- Bell MM, Montgomery MT. 2010. Sheared deep vortical convection in pre-depression *Hagupit* during TCS08. *Geophys. Res. Lett.* **37**: L06802.
- Bryan GH. 2002. 'An investigation of the convective region of numerically simulated squall lines'. PhD thesis, Pennsylvania State University: USA.
- Bryan GH, Fritsch JM. 2002. A benchmark simulation for moist non-hydrostatic numerical models. *Mon. Weather Rev.* **130**: 2917–2928.
- Emanuel KA. 1994. *Atmospheric convection*. Oxford University Press: Oxford, UK.
- Gilmore MS, Straka JM, Rasmussen EN. 2004. Precipitation and evolution sensitivity in simulated deep convective storms: Comparisons between liquid-only and simple ice and liquid phase microphysics. *Mon. Weather Rev.* **132**: 1897–1916.
- Guimond SR, Heymsfield GM, Turk FJ. 2010. Multiscale observations of hurricane *Dennis* (2005): The effects of hot towers on rapid intensification. *J. Atmos. Sci.* **67**: 633–654.
- Hendricks EA, Montgomery MT, Davis CA. 2004. On the role of 'vortical' hot towers in formation of tropical cyclone *Diana* (1984). *J. Atmos. Sci.* **61**: 1209–1232.
- Houze RA, Lee W-C, Bell MM. 2009. Convective contribution to the genesis of hurricane *Ophelia* (2005). *Mon. Weather Rev.* **137**: 2778–2800.
- McCauley EW, Weisman ML. 1996. Simulations of shallow supercell storms in landfalling hurricane environments. *Mon. Weather Rev.* **124**: 408–429.
- Montgomery MT, Smith RK. 2010. 'Tropical cyclone formation: Theory and idealized modelling'. Report for the Seventh International Workshop on Tropical Cyclones, La Réunion, November 2010. World Meteorological Organization: Geneva, Switzerland.
- Montgomery MT, Nicholls ME, Cram TA, Saunders AB. 2006. A vortical hot tower route to tropical cyclogenesis. *J. Atmos. Sci.* **63**: 355–386.
- Nguyen SV, Smith RK, Montgomery MT, Persing J. 2008. Tropical cyclone intensification and predictability in three dimensions. *Q. J. R. Meteorol. Soc.* **134**: 563–582.
- Raymond DJ, López Carillo C. 2011. The vorticity budget of developing typhoon *Nuri* (2008). *Atmos. Chem. Phys.* **11**: 141–163.
- Raymond DJ, Sessions L. 2007. Evolution of convection during tropical cyclogenesis. *Geophys. Res. Lett.* **34**: L06811, DOI: 10.1029/2006GL028607.
- Reasor PD, Montgomery MT, Boast LF. 2005. Mesoscale observations of the genesis of hurricane *Dolly* (1996). *J. Atmos. Sci.* **62**: 3151–3171.
- Rozoff CM. 2007. 'Aspects of moat formation in tropical cyclone eyewall replacement cycles'. PhD thesis, Colorado State University: USA.
- Rozoff CM, Schubert WH, McNoldy B, Kossin JP. 2006. Rapid filamentation zones in intense tropical cyclones. *J. Atmos. Sci.* **63**: 325–340.
- Shin S, Smith RK. 2008. Tropical cyclone intensification and predictability in a minimal three-dimensional model. *Q. J. R. Meteorol. Soc.* **134**: 1661–1671.
- Sippel JA, Nielsen-Gammon JW, Allen SE. 2006. The multiple vortex nature of tropical cyclogenesis. *Mon. Weather Rev.* **134**: 1796–1814.
- Smith RK, Montgomery MT. 2010. Hurricane boundary-layer theory. *Q. J. R. Meteorol. Soc.* **136**: 1665–1670.
- Smith RK, Montgomery MT, Zhu H. 2005. Buoyancy in tropical cyclones and other rapidly rotating vortices. *Dyn. Atmos. Oceans* **40**: 189–208.
- Smith RK, Montgomery MT, Nguyen SV. 2009. Tropical cyclone spin-up revisited. *Q. J. R. Meteorol. Soc.* **135**: 1321–1335.
- Weisman ML, Klemp JB. 1982. The dependence of numerically simulated convective storms on vertical wind shear and buoyancy. *Mon. Weather Rev.* **110**: 504–520.
- Wissmeier U. 2009. 'The physics of tropical convection'. PhD thesis, Ludwig-Maximilians University of Munich: Germany.